PAPER

Check for updates

Microhydration of protonated 5-hydroxyindole revealed by infrared spectroscopy†

Johanna Klyne [ID] and Otto Dopfer [ID] *

Controlled microsolvation of protonated aromatic biomolecules with water is fundamental to understand proton transfer reactions in aqueous environments. We measured infrared photodissociation (IRPD) spectra of mass-selected microhydrates of protonated 5-hydroxyindole (5HIH$^+$–W$_n$, W = H$_2$O, n = 1–3) in the OH and NH stretch ranges (2700–3800 cm^{-1}), which are sensitive to the spectroscopic characteristics of interior solvation, water network formation, and proton transfer to solvent. Analysis of the IRPD spectra by dispersion-corrected density functional theory calculations (B3LYP-D3/aug-cc-pVTZ) reveals the coexistence of C3- and C4-protonated carbenium ions, 5HIH$^+$(C3) and 5HIH$^+$(C4), as well as the O-protonated oxonium ion, 5HIH$^+$(O). Monohydrated 5HIH$^+$–W clusters are formed by hydrogen-bonding (H-bonding) of the first water to the most acidic functional group, namely, the NH group in the case of 5HIH$^+$(C3), the OH group for 5HIH$^+$(C4), and the OH$_2$ group for 5HIH$^+$(O). The latter benefits from its twofold degeneracy and the outstandingly high binding energy of $D_0 \sim$ 100 kJ mol^{-1}. Larger 5HIH$^+$–W$_{2/3}$ clusters preferably grow (i) by H-bonding of the second water to the remaining vacant functional group and and/or (ii) by formation of W$_2$ water chains at the respective most acidic functional group. Our IRPD spectra of 5HIH$^+$–W$_n$ do not indicate any proton transfer to the solvent up to n = 3, in line with the proton affinities of 5HI and W$_n$. Comparison of 5HIH$^+$–W$_n$ to neutral 5HI–W and cationic 5HI$^+$–W$_n$ clusters elucidates the impact of different charge states on the topology of the initial solvation shell. Furthermore, to access the influence of the size of the arene ion and a second functional group, we draw a comparison to microhydration of protonated phenol.

1. Introduction

The interaction of biomolecules, such as proteins, enzymes or hormones, with water (W) is crucial for their structure and function in living organisms. Controlled sequential microhydration of isolated biomolecules facilitates investigation of the interactions between solutes and solvents, which are blurred in the condensed phase. Infrared (IR) vibrational spectroscopy of size-selected hydrated clusters is particularly useful because it provides direct structural information. Combined with quantum chemistry, IR spectroscopy can elucidate the potential energy surface of hydration interactions.

Aromatic heterocyclic molecules are ubiquitous biomolecular building blocks.[1–3] For example, 5-hydroxyindole (5HI), the prototype chosen herein, consists of pyrrole fused to a phenol ring and occurs as a subunit in the neurotransmitter serotonin. The sequential microhydration of protonated aromatic molecules is particularly interesting because proton transfer from the

Institut für Optik und Atomare Physik, Technische Universität Berlin, Hardenbergstr. 36, 10623 Berlin, Germany. E-mail: dopfer@physik.tu-berlin.de; Fax: +49-30-31423018

† Electronic supplementary information (ESI) available. See DOI: 10.1039/c8cp06950f

biomolecule to the solvent may happen in these systems. Both, protonation and hydration are found to enhance the acidity of the functional groups (OH/NH), and hence their ability to donate a proton.[4,5] Moreover, the proton affinity (PA) of W (PA = 691 kJ mol^{-1})[6] and small W$_n$ clusters (PA = 808–879 kJ mol^{-1} for n = 2–3)[7,8] is in the same range as those of aromatic hydrocarbons (*e.g.*, PA = 750 kJ mol^{-1} for benzene).[6] Hence, formation of a hydronium ion (H$_3$O$^+$) or protonated water clusters H$^+$(H$_2$O)$_n$ *via* proton transfer can eventually increase the interaction energy resulting in more stable hydrated clusters. For example, protonated benzene releases its excess proton already upon hydration by a single water molecule.[9,10] Moreover, for the prototypical protonated arenes (A) naphthalene and benzaldehyde, proton transfer to water occurs at cluster sizes of n = 2 and 3, respectively, as revealed from IR photodissociation (IRPD) spectra of their microhydrated [A–W$_n$]H$^+$ clusters.[11,12] In general, the topology of the potential energy surface of hydrated clusters strongly depends on their charge or protonation state.[5,13–15]

The microhydration of the protonated phenol (PhH$^+$) subunit of 5HI has been studied by quantum chemistry and IRPD spectroscopy.[14,16] While the theoretical study focused on the electronic structure of the carbenium ion,[16] the IRPD study indicates the coexistence of *ortho/para* C-protonated carbenium

2706 | *Phys. Chem. Chem. Phys.,* 2019, **21**, 2706–2718

This journal is © the Owner Societies 2019

and O-protonated oxonium isomers, PhH$^+$(o/p) and PhH$^+$(O), in a molecular beam.[14] For both types of protomers, small W$_n$ clusters are formed at the OH group of phenol. However, proton transfer is observed at different critical sizes of the hydration shell (n_c). While the W$_n$ network accepts the excess proton already at $n_c = 3$ for PhH$^+$(O)–W$_n$, proton transfer is only possible for $n \geq 4$ in PhH$^+$(o/p)–W$_n$. This change in n_c is explained by the geometry of the carbenium cluster. The protonated CH$_2$ group is simply too far away from the W$_n$ network at the OH group. Proton transfer is possible only when the W$_n$ cluster forms a ring bridging the OH and CH$_2$ groups at $n_c = 4$. The role of binding energies (D_0) of the PhH$^+$–W$_n$ clusters or differences in the acidity of the OH groups have not been discussed. However, our preceding IRPD study of the sequential microsolvation of protonated 5-hydroxyindole (5HIH$^+$) by nonpolar Ar and quadrupolar N$_2$ ligands (L) indicates a drastic difference in the ligand binding energies of the carbenium and oxonium protomers, 5HIH$^+$(C) and 5HIH$^+$(O).[17] The 5HIH$^+$–L$_n$ spectra ($n \leq 3$) reveal the coexistence of 5HIH$^+$(C3)–L$_n$, 5HIH$^+$(C4)–L$_n$, and 5HIH$^+$(O)–L$_n$ clusters with ion cores protonated at C3, C4, and O, respectively. This finding is surprising at first glance, because bare 5HIH$^+$(O) is drastically less stable than the carbenium ions ($\Delta E_0 > 100$ kJ mol^{-1}).[5,17] The presence of clusters with an oxonium core can however be rationalized by the outstandingly large binding energies of 5HIH$^+$(O)–L$_n$(OH) clusters with ligands attached to the OH$_2$ group, the high barriers for isomerization from the oxonium to the carbenium ions (kinetic trapping), and the twofold degeneracy of these structures.[14,17–20] Furthermore, the acidity of the NH and OH functional groups is found to strongly depend on the protonation site.[17] Comparison with PhH$^+$ indicates an increase in the acidity of the OH group from 5HIH$^+$ to PhH$^+$.[17] Hence, we expect intracluster proton transfer in 5HIH$^+$–W$_n$ clusters for a larger n_c value as compared to PhH$^+$–W$_n$.

To the best of our knowledge, only one theoretical study describes the microhydration of protonated 5HIH$^+$,[5] and the protonation-induced change of the interaction potential compared to neutral hydrated clusters. This study reveals the preference of OH$\cdots$W over NH$\cdots$W H-bonds in the neutral ground state, in line with spectroscopic data.[14] Both, OH$\cdots$W and NH$\cdots$W H-bonds are significantly strengthened upon protonation,[5] whereas the increase in the acidity of the NH group is more pronounced than that of the OH group. As a result, the topology of the hydration shell is changed upon protonation and NH$\cdots$W bonds are preferred. However, only C3-protonated 5HIH$^+$(C3)–W clusters have been considered.[5] Most likely, the topologies of 5HIH$^+$(C4)–W and 5HIH$^+$(O)–W clusters differ strongly.[17] Thus, we address herein three main questions: (i) what is the protomer abundance within 5HIH$^+$–W$_n$ clusters and how is it changed compared to 5HIH$^+$–L$_n$ with L = Ar and N$_2$; (ii) what is the structure of the initial solvation shell in 5HIH$^+$–W$_n$; and (iii) do we observe proton transfer in the size range $n \leq 3$ and a protomer dependence of n_c?

To this end, we analyze IRPD spectra of mass-selected hydrated clusters of 5HIH$^+$ with the aid of quantum chemical calculations. Vibrational spectroscopy in the NH and OH stretch range can determine the protonation site, discriminate interior ion solvation from water network formation, and signal

potential proton transfer from 5HIH$^+$ to the W$_n$ solvent cluster. The comparison of our results on 5HIH$^+$–W to those obtained for 5HI$^+$–W and 5HI–W illustrates the influence of different charge states and protonation on the solvation of 5HI.

2. Experimental and computational techniques

The microsolvation of 5HIH$^+$ is studied by IRPD spectroscopy of mass-selected 5HIH$^+$–W$_n$ ($n = 1$–3) clusters. Additional spectra of colder 5HIH$^+$–W are obtained by Ar and N$_2$ tagging. IRPD spectra are measured in the XH stretch range (X = N and O, 2600–3800 cm^{-1}) with a quadrupole–octopole–quadrupole tandem mass spectrometer described elsewhere.[18–26] Briefly, protonated clusters are generated in an electron ionization source coupled to a pulsed molecular beam expansion. Solid 5HI (Sigma-Aldrich, 97%) is heated to 145 °C and the resulting vapor is seeded in Ar or N$_2$ carrier gas (8–9 bar) containing water. He/H$_2$ gas (90/10) is added to pure Ar (N$_2$) in a 1 : 1 ratio to enhance the protonation efficiency. The gas mixture is expanded into vacuum through a pulsed nozzle. Close to the nozzle orifice, electron and/or chemical ionization of X (X = Ar, N$_2$, H$_2$, or W$_n$) forms XH$^+$ ions, which subsequently protonate 5HI via proton transfer.[18–20,24] Three-body collisions with W and/or carrier gas molecules lead to cluster formation. In the first quadrupole, the desired parent clusters are mass-selected. Pulsed IR radiation emitted from a tunable optical parametric oscillator (2–4 mJ pulse energy, 10 Hz repetition rate, 1 cm^{-1} bandwidth) is introduced into the adjacent octopole. Resonant vibrational excitation of the parent clusters leads to the loss of the least bonded ligand, i.e. single W molecules in the case of 5HIH$^+$–W$_n$ or the loosely bound Ar/N$_2$ tag for 5HIH$^+$–W–Ar/N$_2$. The produced fragment ions are mass-selected with the second quadrupole and monitored by a Daly detector as a function of the IR laser frequency to derive the IRPD spectrum of the 5HIH$^+$–W$_n$ or 5HIH$^+$–W–Ar/N$_2$ parent clusters. The ion source is triggered at 20 Hz (twice the laser frequency) facilitating subtraction of the background signal (metastable decay). All IRPD spectra are normalized for laser intensity variations recorded with a pyroelectric detector. Collision-induced dissociation in the octopole confirms the composition of mass-selected parent clusters.[22,23]

The protonation sites in 5HIH$^+$ have already been examined in a previous study.[17] The 5HIH$^+$ protomers offer two competing H-bonding sites for W molecules, namely, their NH and OH functional groups. The 5HIH$^+$–W$_n$ input structures for geometry optimization are constructed by hand, attaching W ligands successively to the NH and OH groups. Up to $n = 3$, this approach is still feasible to find all low-energy minima. For larger hydrates (and more flexible organic chromophores), it may be rather difficult to find geometries by hand and, as a consequence, systematic computational sampling techniques such as basin-hopping or molecular dynamics should be employed.[28–30] Geometries, energies, and harmonic IR spectra of stable 5HIH$^+$–W$_n$ ($n = 1$–3) and 5HIH$^+$–W–Ar/N$_2$ (ESI†) structures are calculated at the B3LYP-D3/aug-cc-pVTZ level using GAUSSIAN09.[27,31–34] This hybrid density functional with

This journal is © the Owner Societies 2019

Phys. Chem. Chem. Phys., 2019, **21**, 2706–2718 | 2707

additive dispersion correction has proven to yield reliable results for related aromatic clusters.[11,22,23,35–39] For example, the binding energies computed for the monohydrates of the benzene and naphthalene cations (D_0 = 3209 and 2773 cm^{-1}) compare favorably with the experimental values (D_0 = 3290 $\pm$ 120 and 2800 $\pm$ 300 cm^{-1}).[40,41] Similarly, the calculated binding energy of W_2 (D_0 = 1108 cm^{-1}) matches the measured value (D_0 = 1105 $\pm$ 10 cm^{-1}).[42,43] We optimize selected structures also at the PBE0-D3/aug-cc-pVTZ level to yield reference data on structural and spectroscopic properties. The PBE0 functional is frequently used to compute properties of molecular clusters and is less empirical than B3LYP.[28,30,44–46] Furthermore, single-point energy calculations of selected optimized structures are performed at the CC2/aug-cc-pVDZ level. Comparison to neutral and cationic s/a5HI–W clusters previously studied at the same level (B3LYP-D3/aug-cc-pVTZ) yields the effects of protonation.[22,23] Total binding energies (D_0) are derived by subtracting the zero-point corrected energies of the corresponding monomers from that of the cluster: $D_0 = E_0(\text{5HIH}^+\text{–W}_n) - E_0(\text{5HIH}^+) - n \cdot E_0(\text{W})$. Binding energies of the Ar/N$_2$ tag in 5HIH$^+$–W–Ar/N$_2$ are calculated in a similar way. For selected structures, we estimate the basis set superposition errors (BSSE) using the counterpoise method.[47,48] Calculated harmonic vibrational frequencies are linearly scaled by a factor of 0.957 derived previously from fitting the free OH stretching frequency of cationic s/a5HI$^+$.[22] Yet, this scaling factor yields OH stretch frequencies of W ($\nu_{1/3}$ = 3635/3733 cm^{-1}) systematically lower by $\sim$20 cm^{-1} than the experimental values ($\nu_{1/3}$ = 3657/3756 cm^{-1}).[49] For selected 5HIH$^+$–W clusters, anharmonic spectra are calculated at the B3LYP-D3/aug-cc-pVDZ level as implemented in GAUSSIAN09.[50]

3. Results and discussion

3.1 IRPD spectra

An overview of the IRPD spectra of 5HIH$^+$–W$_n$ with n = 1–3 measured in the XH stretch range is given in Fig. 1. The positions, widths, and suggested vibrational and isomer assignments of the transitions observed (A–L, X) are listed in Table 1, along with computed frequencies and IR oscillator strengths. The spectra cover the antisymmetric and symmetric OH stretching modes of water (ν_3 and ν_1, bands A and B) and the OH and NH stretching modes of 5HIH$^+$ (ν_{OH} and ν_{NH}). Dotted lines indicate the correspondence of related bands in the different spectra. Bands G and H emerging in the spectra of 5HIH$^+$–W$_n$ with $n \geq 2$ already indicate the formation of a H-bonded water network. In the following, the IRPD spectra are disentangled by comparison with IR spectra calculated for the possible isomers and taking into account the previous interpretation of the 5HIH$^+$–L$_n$ spectra with L = Ar and N$_2$.[17] IRPD spectra of tagged 5HIH$^+$–W–L clusters with L = Ar and N$_2$ are shown in Fig. S1 in the ESI.†

3.2 5HIH$^+$–W

Internal OH rotation yields *syn* and *anti* rotamers of 5HIH$^+$, denoted by s5HIH$^+$ and a5HIH$^+$, respectively. Our previous study of 5HIH$^+$–L$_n$ demonstrates the coexistence of the most
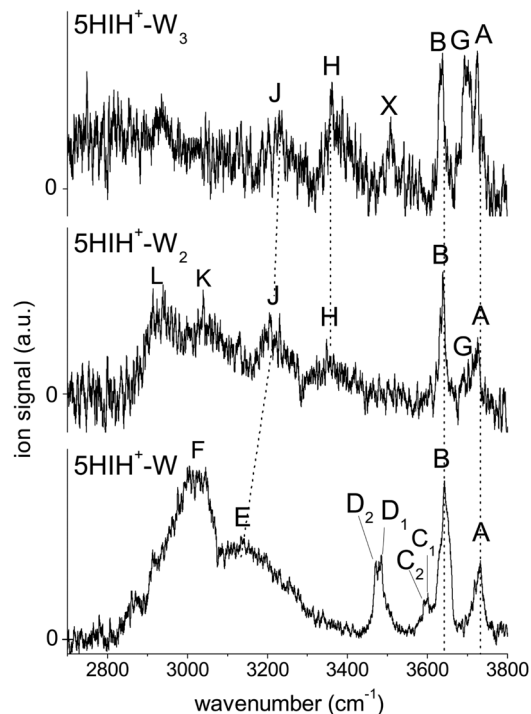

Fig. 1 Overview of the IRPD spectra of 5HIH$^+$–W$_n$ (n = 1–3) measured in the XH stretch range (2700–3800 cm^{-1}). The positions, widths, and vibrational and isomer assignments of the transitions are listed in Table 1.

stable s/a5HIH$^+$(C3) protomers (ΔE_0 = 0/1.8 kJ mol^{-1}), as well as the s/a5HIH$^+$(C4) and s/a5HIH$^+$(O) isomers (ΔE_0 = 5.1/11.1 and 117.1/117.7 kJ mol^{-1}).[17] With the exception of 5HIH$^+$(C4), the *syn* and *anti* rotamers of the 5HIH$^+$ protomers have similar energies and IR spectra and thus cannot be distinguished at the current spectral resolution. A deep potential well (ΔE > 150 kJ mol^{-1}) prevents the interconversion of the drastically less stable 5HIH$^+$(O) isomers into 5HIH$^+$(C4).[17] We compute proton affinities (PAs) of 905/902 kJ mol^{-1} for s/a5HIH$^+$(C3), 900/892 kJ mol^{-1} for s/a5HIH$^+$(C4), and 786/785 kJ mol^{-1} for s/a5HIH$^+$(O).[17] On the other hand, for W$_n$ clusters we calculate PAs of 681, 818, and 898 kJ mol^{-1} for n = 1–3, respectively. Hence, the predicted PA of s/a5HIH$^+$(O) is smaller than that of the W$_n$ cluster already at n = 2, and the proton may be transferred from this 5HIH$^+$ protomer to the W$_n$ solvent cluster. The PAs of s/a5HIH$^+$(C3/C4) are in the same range as that of the W$_3$ cluster. Yet, proton transfer may still occur if the solvation energy of the proton-transferred structure is higher. Due to the possible proton transfer to the W$_n$ moiety, the notation [5HI–W$_n$]H$^+$ is more precise. However, for consistency, we keep the 5HIH$^+$–W$_n$ notation for all clusters throughout this paper. Based on our previous results,[17] we calculate herein hydrated clusters of s/a5HIH$^+$(C3), s/a5HIH$^+$(C4), and s/a5HIH$^+$(O) with W attached to the acidic functional OH$_{(2)}$ and NH groups, the π-electron cloud, or the protonated CH$_2$ group. In general, the binding motifs are very similar for the *syn* and *anti* rotamers of the 5HIH$^+$–W$_n$ clusters, with s5HIH$^+$–W$_n$ being systematically more stable (Table S1, ESI†). Therefore, in the main text and

Table 1 Positions (in cm^{-1}) and widths (FWHM, in parentheses) of the bands observed in the IRPD spectra of 5HIH$^+$–W$_n$ (n = 1–3) (Fig. 1) compared to scaled harmonic frequencies (in cm^{-1}) and IR intensities (km mol^{-1}, in parentheses) of the assigned s5HIH$^+$–W$_n$ isomers calculated at the B3LYP-D3/aug-cc-pVTZ level. Vibrational frequencies of the corresponding a5HIH$^+$–W$_n$ clusters are listed in Table S1 (ESI)

Cluster	Exp.	Vibration	Calc.	Isomer
5HIH$^+$–W	**A** 3732 (30)	ν_3	3704 (119)	s5HIH$^+$(C3)–W(NH)
		ν_3	3708 (118)	s5HIH$^+$(C4)–W(NH)
		ν_3	3697 (134)	s5HIH$^+$(C4)–W(OH)
		ν_3	3685 (178)	s5HIH$^+$(O)–W(OH)
	B 3641 (25)	ν_{OH}^f	3632 (164)	s5HIH$^+$(C3)–W(NH)
		ν_1	3622 (54)	s5HIH$^+$(C3)–W(NH)
		ν_1	3612 (52)	s5HIH$^+$(C4)–W(OH)
		ν_1	3622 (40)	s5HIH$^+$(C4)–W(NH)
		ν_1	3600 (68)	s5HIH$^+$(O)–W(OH)
	C$_1$ 3600 (5)	ν_{OH}^f	3588 (219)	s5HIH$^+$(C4)–W(NH)
	C$_2$ 3591 (5)	ν_{OH}^f	3558 (199)	s5HIH$^+$(O)–W(OH)
	D$_1$ 3485 (30)	ν_{NH}^f	3494 (116)	s5HIH$^+$(O)–W(OH)
	D$_2$ 3470 (30)	ν_{NH}^f	3478 (139)	s5HIH$^+$(C4)–W(OH)
	E 3130 (100)	ν_{NH}^b	3191 (1184)	s5HIH$^+$(C4)–W(NH)
	F 3015 (70)	ν_{OH}^b	3035 (2283)	s5HIH$^+$(C4)–W(OH)
		ν_{NH}^b	3011 (1399)	s5HIH$^+$(C3)–W(NH)
5HIH$^+$–W$_2$	**A** 3725 (20)	ν_3	3711 (131)/3707 (113)	s5HIH$^+$(C3)–W$_2$(NH–OH)
		ν_3	3717 (114)	s5HIH$^+$(C3)–W$_2$(NH–W)
		ν_3	3711 (114)/3700 (128)	s5HIH$^+$(C4)–W$_2$(NH–OH)
	G 3692 (10)	$\nu_{OH}^{f(W)}$	3690 (105)	s5HIH$^+$(C3)–W$_2$(NH–W)
	B 3638 (15)	ν_1	3624 (49)/3619 (33)	s5HIH$^+$(C3)–W$_2$(NH–OH)
		ν_{OH}^f	3635 (156)	s5HIH$^+$(C3)–W$_2$(NH–W)
		ν_1	3624 (37)/3615 (48)	s5HIH$^+$(C4)–W$_2$(NH–OH)
	H 3348 (>50)	ν_{OH}^b	3283 (1565)	s5HIH$^+$(C3)–W$_2$(NH–OH)
		$\nu_{OH}^{b(W)}$	3308 (921)	s5HIH$^+$(C3)–W$_2$(NH–W)
	J 3205 (>50)	ν_{NH}^b	3218 (1094)	s5HIH$^+$(C4)–W$_2$(NH–OH)
	K 3040 (>50)	ν_{NH}^b	3041 (1331)	s5HIH$^+$(C3)–W$_2$(NH–OH)
		ν_{OH}^b	3083 (2234)	s5HIH$^+$(C4)–W$_2$(NH–OH)
	L 2940 (>50)	ν_{NH}^b	2787 (2249)	s5HIH$^+$(C3)–W$_2$(NH–W)
5HIH$^+$–W$_3$	**A** 3725 (20)	ν_3	3719 (112)/3708 (114)	s5HIH$^+$(C3)–W$_3$(OH–NH–W)
		ν_3	3721 (111)	s5HIH$^+$(C3)–W$_3$(NH–W–W)
		ν_3	3722 (208)	s5HIH$^+$(C3)–W$_3$(W–NH–W)
		ν_3	3723 (106)/3702 (127)	s5HIH$^+$(C4)–W$_3$(OH–NH–W)
		ν_3	3722 (115)/3712 (112)	s5HIH$^+$(C4)–W$_3$(OH–W–NH)
		ν_3	3702 (147)/3695 (222)	s5HIH$^+$(O)–W$_3$(NH–OH–W1)
		ν_3	3717 (128)/3704 (143)	s5HIH$^+$(O)–W$_3$(NH–OH–W2)
	G 3692 (30)	ν_{OH}^f	3692 (102)	s5HIH$^+$(C3)–W$_3$(OH–NH–W)
		$\nu_{OH}^{f(W)}$	3694 (70)	s5HIH$^+$(C3)–W$_3$(NH–W–W)
		$\nu_{OH}^{f(W)}$	3693 (111)	s5HIH$^+$(C3)–W$_3$(NH–W–W)
		$\nu_{OH}^{f(W)}$	3689 (92)	s5HIH$^+$(C4)–W$_3$(OH–NH–W)
		$\nu_{OH}^{f(W)}$	3679 (100)	s5HIH$^+$(C4)–W$_3$(OH–W–NH)
		$\nu_{OH}^{f(W)}$	3661 (140)	s5HIH$^+$(O)–W$_3$(NH–OH–W1)
		$\nu_{OH}^{f(W)}$	3677 (97)	s5HIH$^+$(O)–W$_3$(NH–OH–W2)
	B 3637 (20)	ν_1	3630 (27)/3620 (31)	s5HIH$^+$(C3)–W$_3$(OH–NH–W)
		$\nu_{OH}^{f(W)}$	3635 (151)	s5HIH$^+$(C3)–W$_3$(NH–W–W)
		ν_1	3631 (23)	s5HIH$^+$(C3)–W$_3$(NH–W–W)
		ν_{OH}^f	3636 (147)	s5HIH$^+$(C3)–W$_3$(W–NH–W)
		ν_1	3631 (29)	s5HIH$^+$(C3)–W$_3$(W–NH–W)
		ν_1	3632 (24)/3616 (45)	s5HIH$^+$(C4)–W$_3$(OH–NH–W)
		ν_1	3631 (29)/3624 (35)	s5HIH$^+$(C4)–W$_3$(OH–W–NH)
		ν_1	3616 (54)/3586 (100)	s5HIH$^+$(O)–W$_3$(NH–OH–W1)
		ν_1	3628 (36)/3617 (45)	s5HIH$^+$(O)–W$_3$(NH–OH–W2)
	X 3508 (30)	ν_{NH}^f	3497 (108)	s5HIH$^+$(O)–W$_3$(NH–OH–W1)
		ν_{NH}^f	3500 (105)	s5HIH$^+$(O)–W$_3$(NH–OH–W2)
	H 3360 (>50)	$\nu_{OH}^{b(W)}$	3375 (723)	s5HIH$^+$(C4)–W$_3$(OH–NH–W)
		$\nu_{OH}^{b(W)}$	3306 (891)	s5HIH$^+$(C4)–W$_3$(OH–W–NH)
		$\nu_{OH}^{b(W)}$	3326 (867)	s5HIH$^+$(C3)–W$_3$(OH–NH–W)
		ν_{OH}^b	3301 (156)	s5HIH$^+$(C3)–W$_3$(OH–NH–W)
		$\nu_{OH}^{b(W)}$	3378 (663)	s5HIH$^+$(C3)–W$_3$(NH–W–W)
		$\nu_{OH}^{b(as)}$	3424 (380)	s5HIH$^+$(C3)–W$_3$(W–NH–W)
		$\nu_{OH}^{b(s)}$	3381 (516)	s5HIH$^+$(C3)–W$_3$(W–NH–W)

Table 1 (continued)

Cluster	Exp.	Vibration	Calc.	Isomer
J 3230 (>50)		ν_{OH}^{b}	3110 (1927)	$s5HIH^{+}(C4)–W_3(OH–NH–W)$
		ν_{NH}^{b}	3078 (1906)	$s5HIH^{+}(C4)–W_3(OH–NH–W)$
		ν_{NH}^{b}	3236 (1063)	$s5HIH^{+}(C4)–W_3(OH–W–NH)$
		$\nu_{OH}^{b(W)}$	3126 (1404)	$s5HIH^{+}(C3)–W_3(NH–W–W)$
		ν_{OH}^{b}	3183 (1263)	$s5HIH^{+}(O)–W_3(NH–OH–W2)$
		ν_{OH}^{b}	3183 (1263)	$s5HIH^{+}(O)–W_3(NH–OH–W2)$

figures, we concentrate on $s5HIH^{+}–W_n$. Corresponding data for $a5HIH^{+}–W_n$ are available in the ESI.†

Fig. 2 summarizes the calculated $s5HIH^{+}–W$ clusters relevant for the present study, along with their binding and relative energies (D_0, E_0) and intermolecular H-bond lengths (R). Additional geometric and spectroscopic properties are listed in Table S1 (ESI†). Further stable binding motifs of $s5HIH^{+}–W$ are shown in Fig. S2, and corresponding structures of $a5HIH^{+}–W$ are given in Fig. S3 (Table S1, ESI†).
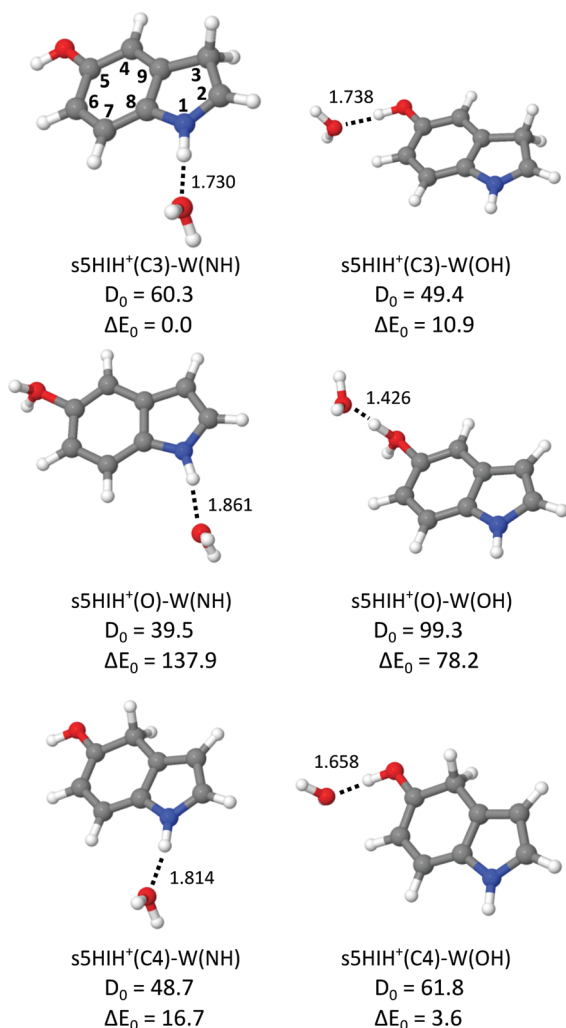

Fig. 2 Structures of selected $s5HIH^{+}–W$ clusters calculated at the B3LYP-D3/aug-cc-pVTZ level (Table S1, ESI†) along with binding energies and relative energies (D_0 and E_0 in kJ mol^{-1}) and intermolecular bond lengths (R in Å).

All $5HIH^{+}$ protomers exhibit competing H-bonding sites, and most important are the acidic functional $OH_{(2)}$ and NH groups acting as proton donors in OH···O and NH···O H-bonds to W. As already observed for related heterocyclic arene cations,[23,36,41,51–53] π-stacking of W is rather unfavorable, e.g., $D_0 = 33.3$ kJ mol^{-1} for $s5HIH^{+}(C3)–W(\pi)$, and thus not considered further. Only one isomer with W attached to the protonated CH_2 group could be located, namely, $s5HIH^{+}(C4)–W(CH)$ with $D_0 = 28.6$ kJ mol^{-1}. Because of the low binding energy of the CH···O H-bonds, this binding motif is also not considered further. Depending on the protonation site, the acidity of the OH and NH functional groups is changed,[17] and the H-bond strengths vary in the same way. For example, the NH group is the strongest proton donor in $s5HIH^{+}(C3)–W(NH)$ ($\Delta E_0 = 0$ and $D_0 = 60.3$ kJ mol^{-1}, $R = 1.730$ Å for NH···O), while the OH group is preferred in $s5HIH^{+}(C4)–W(OH)$ ($\Delta E_0 = 3.6$ and $D_0 = 61.8$ kJ mol^{-1}, $R = 1.658$ Å for OH···O). The OH···O H-bond of the protonated OH_2 oxonium group is outstandingly strong, with $D_0 = 99.3$ kJ mol^{-1} and $R = 1.426$ Å for $s5HIH^{+}(O)–W(OH)$. This strong H-bond and the twofold degeneracy may thus again somewhat compensate for the large energy gap of $\Delta E_0 = 78.2$ kJ mol^{-1} between $s5HIH^{+}(O)–W(OH)$ and the $s5HIH^{+}(C3)–W(NH)$ global minimum. The NH group of the oxonium protomer is a far less acidic than the OH_2 group, with $D_0 = 39.5$ kJ mol^{-1} and $R = 1.861$ Å for the NH···O H-bond in $s5HIH^{+}(O)–W(NH)$. All considered $s5HIH^{+}–W$ isomers are readily distinguishable by their IR spectra in the investigated spectral range (Fig. 3 and Fig. S4, ESI†). Our calculated binding energies of $s5HIH^{+}(C3)–W(NH)$ and $s5HIH^{+}(C3)–W(OH)$, $D_0 = 60.3$ and 49.4 kJ mol^{-1}, are substantially but systematically smaller than the corresponding H-bond energies reported earlier at the RI-MP2/aug-cc-pVDZ level, $D_e = 88.6$ and 76.8 kJ mol^{-1}.[5] Similar to the MP2 results,[5] the single-point energies computed at the CC2/aug-cc-pVDZ level yield the same energy hierarchy as predicted at the B3LYP-D3/aug-cc-pVTZ level, but the spread of relative energies is somewhat larger (Table S1, ESI†). In general, BSSE corrections of the computed binding energies evaluated at the B3LYP-D3/aug-cc-pVTZ level are small (on the order of 1% or less) because the aug-cc-pVTZ basis set is rather large (Table S1, ESI†). Reference calculations at the PBE0-D3/aug-cc-pVTZ level yield energies, structural and spectroscopic properties comparable to those obtained at the B3LYP-D3/aug-cc-pVTZ level (Table S1, ESI†). Indeed, the IR spectra computed at the B3LYP-D3/aug-cc-pVTZ level match somewhat better the experimental spectra (Fig. S5, ESI†).

In Fig. 3 the IRPD spectrum of $5HIH^{+}–W$ is compared to that of cationic $5HI^{+}–W$ and to linear IR absorption spectra calculated for relevant $s5HIH^{+}–W$ isomers (Table 1). The vibrational assignment

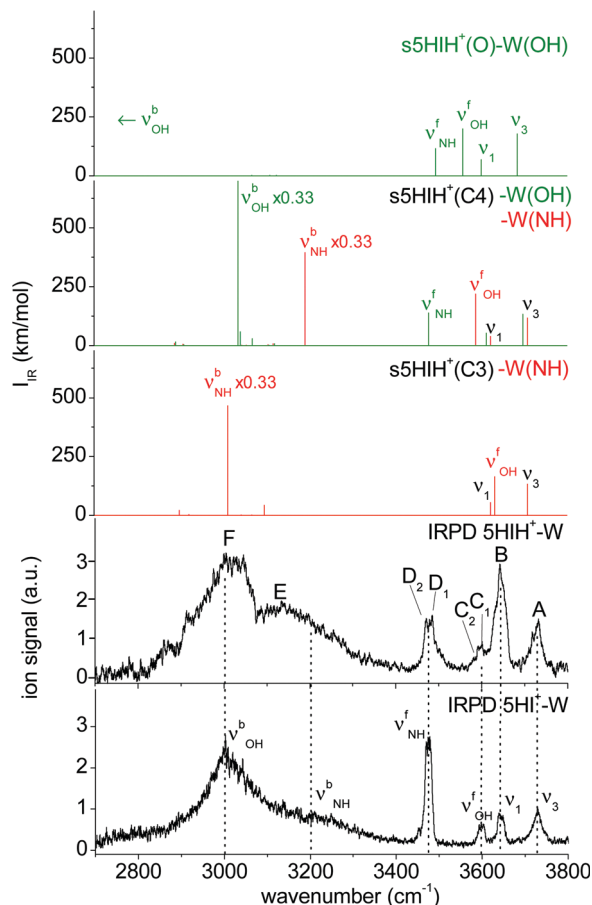**Fig. 3** Comparison of the IRPD spectrum of 5HIH$^+$−W to linear IR spectra calculated for the most stable isomers at the B3LYP-D3/aug-cc-pVTZ level. For comparison, the IRPD spectrum of 5HI$^+$−W is also shown.[23]

is facilitated by comparing the spectra of 5HIH$^+$−W and 5HI$^+$−W. Bands A and B at 3732 and 3641 cm^{-1} are readily assigned to the antisymmetric and symmetric free OH stretching modes of W (ν_3 and ν_1). Band A may also contain the red-shifted ν_3 mode of s5HIH$^+$(O)−W(OH) and s5HIH$^+$(C4)−W(OH) predicted at 3685 and 3697 cm^{-1}, respectively. The relative intensity of band B is substantially enhanced for 5HIH$^+$−W as compared to 5HI$^+$−W, while this is not the case for band A. Some contribution of the free phenolic OH stretching mode (ν_{OH}^f) of s5HIH$^+$(C3)−W(NH) predicted at 3632 cm^{-1} rationalizes the higher intensity of band B. Indeed, comparison of the IRPD spectra of 5HIH$^+$−L with L = Ar, N$_2$, and W further strengthens this assignment.[17] The ν_{OH}^f band of s5HIH$^+$(C3)−Ar(π) is observed at 3635 cm^{-1}, that is only 6 cm^{-1} red-shifted from the maximum of peak B. By comparison to 5HI$^+$−W, bands C$_1$/C$_2$ are clearly assigned to phenolic ν_{OH}^f modes. We attribute C$_1$ at 3600 cm^{-1} to ν_{OH}^f of s5HIH$^+$(C4)−W(NH) predicted at 3588 cm^{-1}, and C$_2$ at 3591 cm^{-1} to ν_{OH}^f of s5HIH$^+$(O)−W(OH) predicted at 3558 cm^{-1}. Another indication for the production of s5HIH$^+$(O)−W(OH) is the doublet D$_1$/D$_2$ at 3485/3470 cm^{-1} ($\Delta\nu$ = 15 cm^{-1}). By analogy to 5HI$^+$−W, it is assigned to the free NH stretching mode (ν_{NH}^f). Here, D$_1$ is attributed to s5HIH$^+$(O)−W(OH) and D$_2$ to s5HIH$^+$(C4)−W(OH) predicted at 3494 and 3478 cm^{-1} ($\Delta\nu$ = 16 cm^{-1}), respectively.

The broad band E centered at 3130 cm^{-1} is interpreted as H-bonded NH stretch (ν_{NH}^b) of s5HIH$^+$(C4)−W(NH) predicted at 3191 cm^{-1}. Band E is somewhat red-shifted compared to ν_{NH}^b in the IRPD spectrum of cationic 5HI$^+$−W, indicating a destabilization of the NH bond induced by C4-protonation. The broad transition F at 3015 cm^{-1} contains both ν_{OH}^b of s5HIH$^+$(C4)−W(OH) and ν_{NH}^b of s5HIH$^+$(C3)−W(NH) predicted at 3035 and 3011 cm^{-1}. The IRPD spectrum shows no clear signature of the s5HIH$^+$(C3)−W(OH) isomer (Fig. S4, ESI†). This finding is somewhat surprising because this isomer is predicted to be slightly more stable than s5HIH$^+$(C4)−W(NH) (ΔE_0 = 10.9 and D_0 = 49.4 kJ mol^{-1} vs. ΔE_0 = 16.7 and D_0 = 48.7 kJ mol^{-1}). We also rule out the presence of the s5HIH$^+$(O)−W(NH) isomer, mostly on the basis of stability and spectroscopy (Fig. S4, ESI†).

In conclusion, we assign the measured IRPD spectrum of 5HIH$^+$−W to C3-protonated s5HIH$^+$(C3)−W(NH) with NH-bonded W, C4-protonated s5HIH$^+$(C4)−W(OH) and s5HIH$^+$(C4)−W(NH) with OH- and NH-bonded W, and the OH-bonded s5HIH$^+$(O)−W(OH) oxonium ion. This interpretation is strengthened by a comparison of the IRPD spectrum to exemplary anharmonic spectra computed for the monohydrates (Fig. S6 and Table S1, ESI†). Obviously, within the harmonic approximation, the red-shifts of the H-bond donor stretching vibrations (ν_{OH}^b and ν_{NH}^b) are underestimated by 60–110 cm^{-1}, but both the anharmonic and scaled harmonic spectra yield the same assignment of the experimental transitions. At the current experimental resolution, we cannot discriminate syn and $anti$ rotamers but assume that both are present in significant abundance for the assigned isomers. The estimation of population ratios for the three protomers (C3, C4, O) based on the comparison of measured and computed band intensities is not straightforward due to overlapping transitions. Furthermore, the binding energies of the 5HIH$^+$−W clusters are higher than the IR photon energies in the XH stretch range, such that absorption of a single photon will not lead to fragmentation from cold clusters. Hence, multiple-photon effects or ions with high internal energy must be considered. Moreover, due to the very different binding energies of the individual 5HIH$^+$−W clusters, the photodissociation cross sections may be different, too. Still, assuming similar fragmentation cross sections for the assigned isomers, a rough estimate of populations is possible. In contrast to the predictions for s5HIH$^+$(O)−W(OH), band C (C$_1$ + C$_2$, ν_{OH}^f) is significantly less intense than D (D$_1$ + D$_2$, ν_{NH}^f). This result suggests that we probe only a few oxonium ions ($\sim$10%), while the main contribution to band D arises from s5HIH$^+$(C4)−W(OH). The comparison of bands C and D also indicates that significantly fewer s5HIH$^+$(C4)−W(NH) than s5HIH$^+$(C4)−W(OH) isomers are probed. Band B is roughly twice as intense as band A, while ν_1 is predicted to be half as intense as ν_3 in any of the calculated IR spectra. Thus, we conclude that most signals of band B stem from ν_{OH}^f of s5HIH$^+$(C3)−W(NH). Hence, we suggest that the major contribution (roughly 70%) to the IRPD spectrum arises from the most stable s5HIH$^+$(C3)−W(NH) and s5HIH$^+$(C4)−W(OH) isomers.

3.3 5HIH$^+$−W−Ar/N$_2$

Tagging with Ar or N$_2$ reduces the peak widths in the IRPD spectra of 5HIH$^+$−W because the binding energy of the least

This journal is © the Owner Societies 2019

Phys. Chem. Chem. Phys., 2019, **21**, 2706–2718 | **2711**

bonded ligand limits the internal temperature of the cluster. Fig. S7 and S8 (ESI†) compare the IRPD spectra of 5HIH⁺–W–Ar and 5HIH⁺–W–N₂ to the IR spectra calculated for relevant tagged isomers. The IRPD spectra of 5HIH⁺–W–Ar/N₂ do not add any new information about the monohydrated clusters but confirm the assignment of s5HIH⁺(C3)–W(NH), s5HIH⁺(C4)–W(OH), s5HIH⁺(C4)–W(NH) and s5HIH⁺(O)–W(OH) being the predominant monohydrates in the molecular beam. The Ar tag is mainly attached to the W moiety or π-stacked. The N₂ ligand is H-bonded to either W or to the remaining functional group not occupied by W.

Selected structures of s5HIH⁺–W–Ar and s5HIH⁺–W–N₂ are depicted in Fig. S9 and S10 (ESI†), respectively, and Table S1 (ESI†) contains structural and spectroscopic information for all calculated 5HIH⁺–W–Ar/N₂ isomers. For a detailed discussion of the 5HIH⁺–W–L spectra, the interested reader is referred to the ESI.†

3.4 5HIH⁺–W₂

Fig. 4 shows the structures of selected s5HIH⁺–W₂ clusters along with binding energies and H-bond lengths. Additional
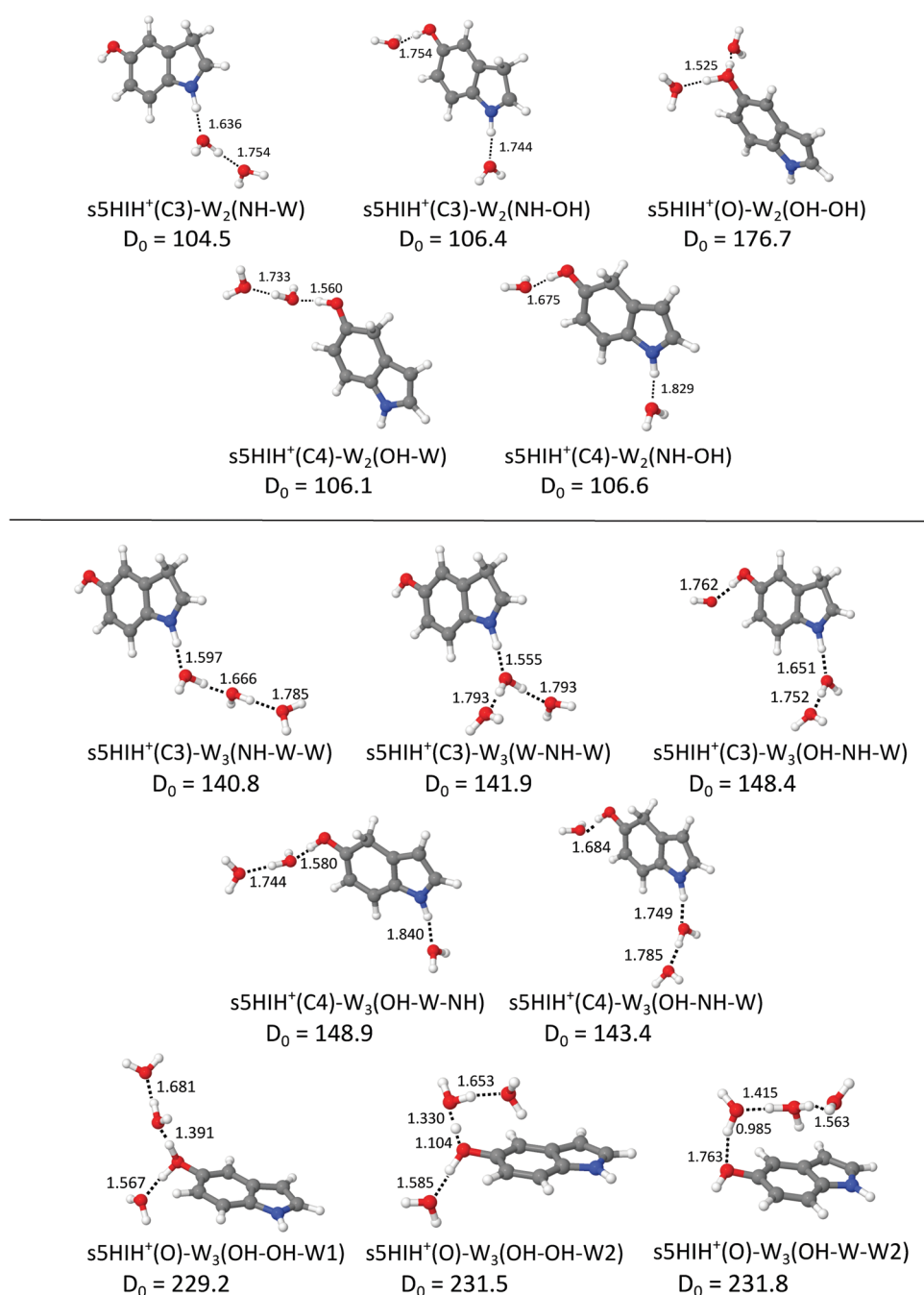

Fig. 4 Structures of selected s5HIH⁺–W_{2/3} clusters calculated at the B3LYP-D3/aug-cc-pVTZ level (Table S1, ESI†) along with binding energies (D_0 in kJ mol^{-1}) and intermolecular distances (R in Å).

2712 | Phys. Chem. Chem. Phys., 2019, 21, 2706–2718

This journal is © the Owner Societies 2019

stable $s5HIH^+-W_2$ isomers are shown in Fig. S11 (ESI†). Corresponding $a5HIH^+-W_2$ structures are depicted in Fig. S12 (ESI†). Selected structural and spectroscopic properties of all calculated $s/a5HIH^+-W_2$ isomers are listed in Table S1 (ESI†).

For $5HIH^+(C3/C4)-W_2$, we consider three binding motifs. H-bonding of two individual W ligands to both functional groups yields the most stable $s5HIH^+(C3/C4)-W_2(NH-OH)$ with $D_0 = 106.4/106.6$ kJ mol^{-1}. BSSE corrections are again on the order of 1% of the computed binding energies (Table S1, ESI†). Noncooperative three-body effects weaken the individual H-bonds compared to the monohydrates, as revealed by comparison of binding energies and H-bond lengths. For example, corresponding H-bonds elongate from $R = 1.730$ and 1.738 Å in $s5HIH^+(C3)-W(NH)$ and $s5HIH^+(C3)-W(OH)$ to $R = 1.744$ and 1.754 Å in $s5HIH^+(C3)-W_2(NH-OH)$. The same trend holds for $s5HIH^+(C4)-W_2(NH-OH)$ with $R = 1.814$ and 1.658 Å compared to $R = 1.829$ and 1.675 Å. This weakening of the H-bonds directly translates into reduced complexation-induced redshifts of the corresponding ν_{NH}^b and ν_{OH}^b modes (Table S1, ESI†). For example, ν_{NH}^b of $s5HIH^+(C3)-W(NH)$ is predicted at 3011 cm^{-1} and that of $s5HIH^+(C3)-W_2(NH-OH)$ at 3041 cm^{-1}. For the C3-protonated ion, formation of a H-bonded water network (*i.e.*, attachment of a H-bonded W_2) at the NH group is more favorable than at the OH group, with $D_0 = 104.5$ and 86.8 kJ mol^{-1} for $s5HIH^+(C3)-W_2(NH-W)$ and $s5HIH^+(C3)-W_2(OH-W)$, respectively. Due to cooperativity, the initial H-bond is shortened from $R = 1.730$ Å in $s5HIH^+(C3)-W(NH)$ to 1.636 Å in $s5HIH^+(C3)-W_2(NH-W)$. In line with the altered acidity of the functional groups for the C4-protonated ion,[17] $s5HIH^+(C4)-W_2(OH-W)$ is more stable than $s5HIH^+(C4)-W_2(NH-W)$, with $D_0 = 106.1$ and 87.6 kJ mol^{-1}, respectively. Again, network formation strengthens the first H-bond with $R = 1.658$ Å in $s5HIH^+(C4)-W(OH)$ *vs.* 1.560 Å in $s5HIH^+(C4)-W_2(OH-W)$. Formation of water networks yields characteristic spectroscopic features, most prominently, $\nu_{OH}^{f(W)}$ and $\nu_{OH}^{b(W)}$ of the solvated water in the W_2 unit, predicted at 3690 and 3307 cm^{-1} for $s5HIH^+(C3)-W_2(NH-W)$. The corresponding ν_3 and ν_1 of the terminal free water are blue-shifted from 3708 and 3622 cm^{-1} in $s5HIH^+(C3)-W(NH)$ to 3717 and 3628 cm^{-1} in $s5HIH^+(C3)-W_2(NH-W)$. The impact on the respective functional group by solvation with W_2 is largely enhanced. For example, ν_{OH}^b of $s5HIH^+(C4)-W_2(OH)$ is predicted at 3035 cm^{-1} and shifts down to 2710 cm^{-1} for $s5HIH^+(C4)-W_2(OH-W)$.

The largest binding energy of $D_0 = 176.7$ kJ mol^{-1} is calculated for $s5HIH^+(O)-W_2(OH-OH)$, *i.e.* the oxonium ion monohydrated at both OH groups. Yet, due to noncooperativity, this value is significantly lower than twice the binding energy of $s5HIH^+(O)-W(OH)$, $D_0 = 99.3$ kJ mol^{-1}. Formation of a water network at the OH_2 group yields $s5HIH^+(O)-W_2(OH-W1)$ and $s5HIH^+(O)-W_2(OH-W2)$ with $D_0 = 167.3$ and 169.7 kJ mol^{-1} (Fig. S11, ESI†). The NH group of the oxonium ion is far less attractive, leading to $s5HIH^+(O)-W_2(NH-OH)$ and $s5HIH^+(O)-W_2(NH-W)$ with only $D_0 = 135.5$ and 73.4 kJ mol^{-1}. Again, BSSE corrections are on the order of only 1% of the computed binding energies (Table S1, ESI†). In $s5HIH^+(O)-W_2(OH-W1)$, the water chain points away from the phenol ring. Proton transfer

to the W_2 chain is indicated, because the OH bond of $s5HIH^+(O)$ is already longer ($r_{OH} = 1.262$ Å) than the OH$\cdots$W bond ($R = 1.147$ Å). Thus, the ion may be better described by $s5HI-H_5O_2^+$. Yet, for consistency, we keep the introduced notation for the structures. On the other hand, in $s5HIH^+(O)-W_2(OH-W2)$ the water chain is bent toward the aromatic ring facilitating an additional OH$\cdots\pi$ interaction with the aromatic π-electron cloud. In this structure, proton transfer is more pronounced, with $r_{OH} = 1.434$ and $R = 1.056$ Å.

The assignment of the IRPD spectrum of $5HIH^+-W_2$ (Table 1) is based on the comparison to the corresponding calculated spectra (Fig. 5 and Fig. S13, ESI†). Exemplary anharmonic spectra depicted in Fig. S14 (ESI†) are in line with the following assignments based on the harmonic spectra. Bands A and B at 3725 and 3638 cm^{-1} are readily assigned to ν_3 and ν_1 and are well reproduced by essentially all considered isomers. Band G at 3692 cm^{-1} is characteristic of an H-bonded W_2 network and appears at 3690 and 3676 cm^{-1} in the calculated spectra of $s5HIH^+(C3)-W_2(NH-W)$ and $s5HIH^+(C4)-W_2(OH-W)$, respectively. In line with the assignments above, ν_{OH}^f of $s5HIH^+(C3)-W_2(NH-W)$ predicted at 3635 cm^{-1} contributes to band B, which is again significantly more intense than band A. The ν_{NH}^f mode characteristic of $s5HIH^+(C4)-W_2(OH-W)$ at 3481 cm^{-1} is however not observed. Hence, we assign only $s5HIH^+(C3)-W_2(NH-W)$. Consequently, band H centered at 3348 cm^{-1} is attributed to a superposition of ν_{OH}^b of $s5HIH^+(C3)-W_2(NH-OH)$ predicted at

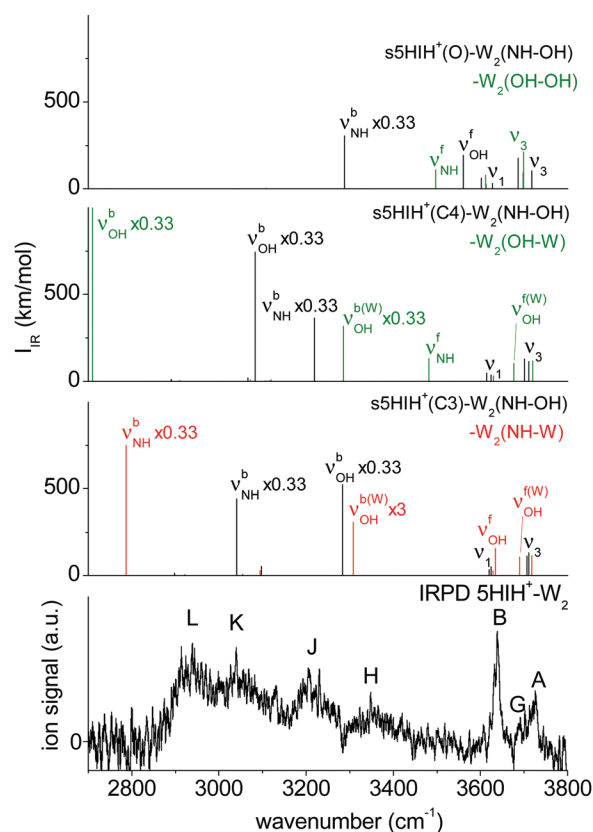**Fig. 5** Comparison of the IRPD spectrum of $5HIH^+-W_2$ to calculated IR spectra of the relevant isomers at the B3LYP-D3/aug-cc-pVTZ level.

This journal is © the Owner Societies 2019

Phys. Chem. Chem. Phys., 2019, **21**, 2706–2718 | **2713**

3283 cm^{-1} and ν_{OH}^b of the W$_2$ unit in s5HIH$^+$(C3)–W$_2$(NH–W), which is predicted at 3308 cm^{-1} ($\nu_{OH}^{b(W)}$). Band J at 3205 cm^{-1} arises from $\nu_{NH}^{b(W)}$ of s5HIH$^+$(C4)–W$_2$(NH–OH) predicted at 3218 cm^{-1}. Its ν_{OH}^b mode at 3083 cm^{-1} and ν_{NH}^b of s5HIH$^+$(C3)–W$_2$(NH–OH) predicted at 3041 cm^{-1} account for band K observed at 3040 cm^{-1}. Finally, band L at 2940 cm^{-1} may be assigned to ν_{NH}^b of s5HIH$^+$(C3)–W$_2$(NH–W), which is predicted to be rather low (2787 cm^{-1}). However, below 2800 cm^{-1}, the laser power is very low such that this mode may also not be detected. We cannot safely assign any 5HIH$^+$(O)–W$_2$ oxonium isomer because there is no strong signal in the IRPD spectrum around 3500 cm^{-1}. In this range, the ν_{NH}^f and ν_{OH}^f modes of s5HIH$^+$(O)–W$_2$(OH–OH) and s5HIH$^+$(O)–W$_2$(NH–OH) are predicted (3498 and 3560 cm^{-1}, Fig. 5). Furthermore, the ν_{NH}^f modes of the two proton-transferred structures s5HIH$^+$(O)–W$_2$(OH–W1) and s5HIH$^+$(O)–W$_2$(OH–W2) and their intense ν_{OH}^b modes of the H-bonded W$_2$ are expected around 3500 cm^{-1} (Fig. S13, ESI†). For the 5HIH$^+$–W cluster, the population of the OH-bound oxonium isomer s5HIH$^+$(O)–W(OH) was most likely enhanced by its high binding energy of D_0 = 99.3 kJ mol^{-1} and the twofold degeneracy. However, degeneracy effects no longer promote the most stable s5HIH$^+$(O)–W$_2$(OH–OH) cluster or the formation of W$_2$ chains in s5HIH$^+$(O)–W$_2$(OH–W1/W2). Thus, our spectra do not indicate proton transfer for any of the 5HIH$^+$–W$_n$ clusters at n = 2.

3.5 5HIH$^+$–W$_3$

In s/a5HIH$^+$–W$_3$, interior ion solvation competes with water network formation. W$_3$ chains at either one of the functional groups (NH–W–W and OH–W–W) are comparably strong as bifurcated W$_3$ H-bonds (W–NH–W and W–OH–W). Selected structures of s5HIH$^+$–W$_3$ are shown in Fig. 4. Additional s5HIH$^+$–W$_3$ and selected a5HIH$^+$–W$_3$ isomers are depicted in Fig. S15 and S16 (ESI†). Corresponding structural and spectroscopic data are listed in Table S1 (ESI†). Again, we observe a strong modulation in the acidity of the functional groups depending on the protonation site. As the NH group is more acidic in s5HIH$^+$(C3), formation of W$_3$ networks at the NH site ($D_0 \approx$ 141 kJ mol^{-1}) is favored over the OH site ($D_0 \approx$ 119 kJ mol^{-1}). The bifurcated W–NH–W H-bond (D_0 = 141.9 kJ mol^{-1}) is slightly favored over the linear NH–W–W chain (D_0 = 140.8 kJ mol^{-1}). However, interior ion solvation with one water molecule attached to the OH group and two to the NH group yields the most stable s5HIH$^+$(C3)–W$_3$(OH–NH–W) isomer with D_0 = 148.4 kJ mol^{-1}. In contrast, W$_3$ networks at the OH site are preferred for s5HIH$^+$(C4) with $D_0 \approx$ 142–145 kJ mol^{-1} (Table S1, ESI†). Solvation of both functional groups yields s5HIH$^+$(C4)–W$_3$(OH–W–NH) and s5HIH$^+$(C4)–W$_3$(OH–NH–W) with D_0 = 148.9 and 143.4 kJ mol^{-1} (Fig. 4). Noncooperative effects destabilize the individual W$_2$ chains. For example, comparing s5HIH$^+$(C4)–W$_2$(OH–W) and s5HIH$^+$(C4)–W$_3$(OH–W–NH), the H-bonds within the W$_2$ chain at the OH group elongate from R = 1.560/1.733 to 1.580/1.744 Å. The same trend is observed for all four interior solvated s5HIH$^+$–W$_3$ isomers (Fig. 4 and Table S1, ESI†). In line with the weakening of the individual H-bonds, for n = 3 (interior solvation) the impact on the s5HIH$^+$ core is also weaker than for n = 2 (water chain).

This directly translates into blue-shifts of the affected proton donor XH stretches. For instance, ν_{NH}^b of s5HIH$^+$(C3)–W$_2$(NH–W) and s5HIH$^+$(C3)–W$_3$(OH–NH–W) are predicted at 2787 and 2834 cm^{-1}, respectively.

Solvation of both OH groups of the oxonium ion yields s5HIH$^+$(O)–W$_3$(OH–OH–W1) and s5HIH$^+$(O)–W$_3$(OH–OH–W2) isomers with D_0 = 229.2 and 231.5 kJ mol^{-1}, respectively. The latter is again stabilized by its additional interaction with the aromatic π-electron cloud. A W$_2$ chain is attached to one OH site, significantly elongating the affected OH bond (r_{OH} = 1.068 and 1.104 Å). The OH···W bond is still longer (R = 1.391 and 1.330 Å). Hence, in contrast to what has been predicted for the corresponding s5HIH$^+$(O)–W$_2$(OH–W1) and s5HIH$^+$(O)–W$_2$(OH–W2) clusters, the proton is not transferred due to the noncooperative character of this W$_3$ binding motif. However, proton-transferred structures cannot be neglected for n = 3. We find four proton-transferred structures, namely, s5HIH$^+$(O)–W$_3$(NH–OH–W1/W2) with a W$_2$ chain at one OH group and a single W at the NH group as well as s5HIH$^+$(O)–W$_3$(OH–W–W1/W2) with a W$_3$ chain at its OH group (Fig. 4 and Fig. S15, ESI†). Interestingly, s5HIH$^+$(O)–W$_3$(OH–W–W2) is the most stable structure found with D_0 = 231.8 kJ mol^{-1}. The W$_3$ chain is entirely detached from the OH group (r_{OH} = 1.763 and $R_{OH–W}$ = 0.985 Å), and is arranged over the phenol ring of neutral 5HI (Fig. 4). This isomer is distinguished by its ν_{OH}^f and ν_{NH}^f predicted at 3633 and 3497 cm^{-1}, and three intense $\nu_{OH}^{b(W)}$ at 3300, 3243, and 2806 cm^{-1}. The other three structures are significantly less stable with D_0 = 201.9, 208.8, and 216.5 kJ mol^{-1}, respectively.

Fig. 6 compares the IRPD spectrum of 5HIH$^+$–W$_3$ to the calculated IR spectra of selected s5HIH$^+$–W$_3$ isomers. Spectra calculated for some additional s/a5HIH$^+$–W$_3$ conformers are given in Fig. S17 (ESI†). The triplet A, G, and B at 3725, 3692, and 3637 cm^{-1} unambiguously reveals the predominance of chainlike W$_2$ and/or W$_3$ solvation structures. Band A is thus assigned to ν_3, band B to ν_1, and band G to $\nu_{OH}^{f(W)}$ of the single-donor water molecules. Candidates to explain this pattern are at least the isomers considered in Fig. 6, except for s5HIH$^+$(C3)–W$_3$(W–NH–W) with a bifurcated H-bond. However, a clear isomer assignment is challenging, because the IRPD spectrum is not well resolved below 3600 cm^{-1}, possibly due to overlapping transitions of several isomers. Still, we can draw some conclusions from the comparison with the IRPD spectra of 5HIH$^+$–W$_{1/2}$ (Fig. 1). First, band X at 3508 cm^{-1} is considered to be a contamination band. It is not convincingly rationalized by any calculated mode and it occurs at the same position as band X in the spectrum of 5HIH$^+$–W–N$_2$ (ESI†). Yet, one may argue that ν_{NH}^f of s5HIH$^+$(O)–W$_3$(NH–OH–W1/W2) predicted at 3497/3500 cm^{-1} gives rise to band X. However, already for 5HIH$^+$–W$_2$ it remains unclear whether oxonium clusters are probed. Any other modes of s5HIH$^+$(O)–W$_3$(NH–OH–W1/W2) are also not clearly observed. Second, bands H and J at 3360 and 3230 cm^{-1} can be related to corresponding transitions in the IRPD spectra of 5HIH$^+$–W$_{1/2}$. In analogy to the spectrum of 5HIH$^+$–W$_2$, band H may be assigned to $\nu_{OH}^{b(W)}$ of the solvated water and/or ν_{OH}^b of the 5HIH$^+$(C3) protomer. Corresponding transitions are predicted at 3225 and 3301 cm^{-1} for s5HIH$^+$(C3)–W$_3$(OH–NH–W). In the

2714 | *Phys. Chem. Chem. Phys.*, 2019, **21**, 2706–2718
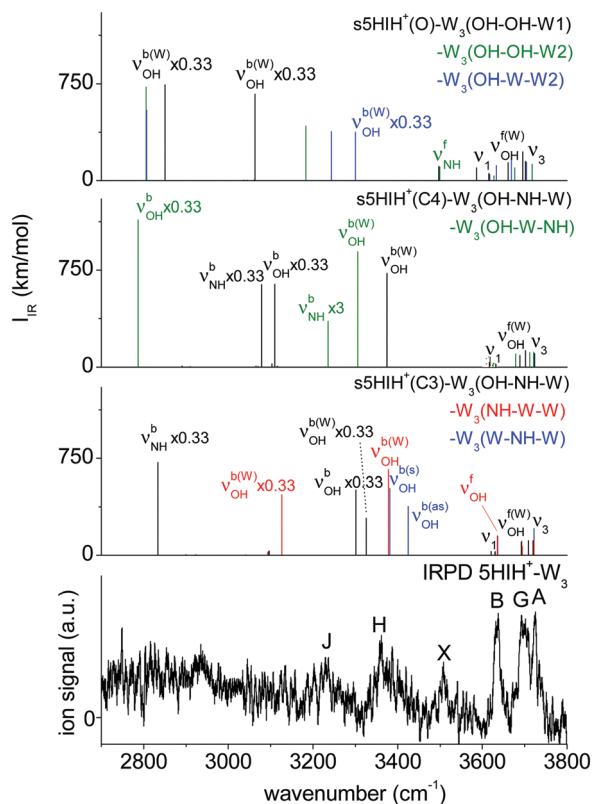
This journal is © the Owner Societies 2019

Fig. 6 Comparison of the IRPD spectrum of 5HIH$^+$–W$_3$ to calculated IR spectra of the relevant isomers at the B3LYP-D3/aug-cc-pVTZ level.

case of 5HIH$^+$–W$_2$, band J is assigned to ν_{NH}^b of the 5HIH$^+$(C4) core. The corresponding intense ν_{NH}^b mode of s5HIH$^+$(C4)–W$_3$(OH–W–NH) is predicted at 3236 cm^{-1}. Bands J and H may also be explained by the two intense $\nu_{OH}^{b(W)}$ of the very stable proton-transferred s5HIH$^+$(O)–W$_3$(OH–W–W2) oxonium isomer, which are predicted at 3300 and 3243 cm^{-1}. Still, the IRPD spectrum of 5HIH$^+$–W$_3$ is already well reproduced by the two most stable carbenium ions s5HIH$^+$(C3)–W$_3$(OH–NH–W) and s5HIH$^+$(C4)–W$_3$(OH–W–NH). Finally, probably due to overlapping bands of several isomers, the spectral resolution is not sufficient to definitely exclude any of the isomers considered in Fig. 6 based on their IR spectra. A suggested, detailed assignment of the observed bands to vibrational modes and isomers is listed in Table 1. We most likely do not observe proton-transferred structures for n = 3, or at most only at low percentage. To unambiguously evidence whether proton transfer happens at n = 3 or not, the isomer contribution must be disentangled more accurately by double-resonance spectroscopy.

3.6 Comparison to 5HIH$^+$–L$_n$ (L = Ar, N$_2$)

Recently, we studied the sequential microsolvation of 5HIH$^+$ with nonpolar (L = Ar) and quadrupolar (L = N$_2$) solvents.[17] The IRPD spectra of the 5HIH$^+$–L clusters with L = Ar, N$_2$, and W are compared in Fig. S18 (ESI†).

The same protomers have been identified in the 5HIH$^+$–L$_n$ clusters, namely, C3, C4 and O. C4-Protonation significantly affects the adjacent OH group. As a result, s- and a5HIH$^+$(C4)

rotamers are distinguishable by their well-resolved ν_{OH}^f bands appearing in the spectra of 5HIH$^+$–Ar and 5HIH$^+$–N$_2$. In contrast, the current 5HIH$^+$–W$_n$ spectra are not sufficiently well resolved to distinguish s- and a5HIH$^+$ rotamers. O-Protomers have unambiguously been identified by the IRPD spectra of larger 5HIH$^+$–(N$_2$)$_{2/3}$ clusters recorded in different fragmentation channels.[17] While the IRPD spectra measured in the $n \rightarrow 0$ loss channel correspond to the superposition of all three protomers, $2 \rightarrow 1$ and $3 \rightarrow 2$ loss channels provide the isomer-pure spectrum of O-protonated 5HIH$^+$(O)–(N$_2$)$_{2/3}$ clusters.

In general, the growth of 5HIH$^+$–L$_n$ clusters (L = Ar, N$_2$, W) follows similar trends. Our previous study related the acidity of the functional groups to the charge distribution in the individual protomers.[17] In 5HIH$^+$(C3) the NH group is most acidic, whereas in 5HIH$^+$(C4) it is the OH group. For the oxonium, exclusively H-bonding to its OH$_2$ group is observed due to its high binding energies of D_0 = 15.2 (Ar), 29.8 (N$_2$), and 99.3 (W) kJ mol^{-1} compared to only D_0 = 5.5 (Ar), 9.3 (N$_2$), and 39.5 (W) kJ mol^{-1} for the NH-bound minimum. H-bonding and π-stacking compete in the growth of 5HIH$^+$–Ar$_n$ clusters. In contrast, the microsolvation of 5HIH$^+$ with N$_2$ is dominated by H-bonding to the functional groups instead of π-stacking, and the same is true for microhydration with W. The L–L interaction is rather small for both Ar and N$_2$ ($\sim$100 cm^{-1}),[54,55] because it relies mainly on dispersion. Hence, their 5HIH$^+$–L$_n$ clusters strongly prefer interior ion solvation over the formation of solvent networks. In contrast, the permanent dipole moment of W promotes the formation of water networks as the W–W interaction is rather strong ($\sim$1000 cm^{-1}).[42,51,52] Upon network formation, strong cooperative effects strengthen preexisting H-bonds, in particular in the presence of a positive charge. Indeed, the formation of W$_2$ and W$_3$ chains is indicated by the characteristic triplet of ν_3, $\nu_{OH}^{f(W)}$, and ν_1 in the IRPD spectra of 5HIH$^+$–W$_{2/3}$. Complexation-induced frequency red-shifts ($\Delta\nu_{XH}$) of H-bonded proton donor stretching modes are a convenient measure of intermolecular H-bond strengths. Therefore, we evaluate the $\Delta\nu_{OH}^b$ and $\Delta\nu_{NH}^b$ red-shifts (Table 2) observed in 5HIH$^+$–L dimers as a function of the ligand (L = Ar, N$_2$, W). Fig. S19 (ESI†) illustrates the dependence of the $\Delta\nu_{OH}^b$ and $\Delta\nu_{NH}^b$ red-shifts on the PAs of the ligands.[6] Generally, the impact on the proton donor group increases monotonically in the order Ar < N$_2$ < W. The $\Delta\nu_{OH}^b$ red-shifts are larger than the $\Delta\nu_{NH}^b$ ones. However, one must be careful with their direct comparison because only for s/a5HIH$^+$(C4) both $\Delta\nu_{OH}^b$ and $\Delta\nu_{NH}^b$ are observed (Table 2). Our previous IRPD study of 5HIH$^+$–Ar/N$_2$ already revealed an increase of the acidity of the OH group in the order s5HIH$^+$(C3) < a5HIH$^+$(C4) < s5HIH$^+$(C4) < s/a5HIH$^+$(O).[17] Indeed, complexation has the largest impact on the OH group of s/a5HIH$^+$(O)–L, which is the strongest H-bond donor with D_0 = 15.2, 29.8, and 61.8 kJ mol^{-1} for Ar, N$_2$, and W, respectively.

3.7 Comparison to neutral 5HI–W and cationic 5HI$^+$–W$_n$

A direct comparison of the (structural) properties of neutral 5HI–W and cationic 5HI$^+$–W to the protonated 5HIH$^+$–W clusters is challenging because protonation strongly affects the chemical structure. While only two isomers, namely, *syn* and *anti* rotamers, exist in the S$_0$ and D$_0$ states of 5HI$^{(+)}$, we observe (at least) six

Table 2 Observed frequencies of the proton donor stretching modes (ν_{XH}, X = N/O, in cm^{-1}) of 5HIH$^+$ and PhH$^+$ and corresponding complexation-induced frequency red shifts ($\Delta\nu_{XH}$) in 5HIH$^+$/PhH$^+$–L clusters (L = Ar, N$_2$, W)

Isomer	ν_{XH}	$\Delta\nu_{XH}$ L = Ar	L = N$_2$	L = W
PhH$^+$(O)	3552 (X = O)[a]	−18[a]	−9[a]	+33[d]
	3477 (X = O)[a]	−148[a]	−440[a]	>−877[d]
PhH$^+$(o/p)	3554 (X = O)[b]	−61	−146	−654
a/s5HIH$^+$(O)	3555 (X = O)[c]	−20	−15	+36
	3480 (X = O)[c]	−115	−335	−1304[c]
	3503 (X = N)	Not observed	Not observed	Not observed
s5HIH$^+$(C3)	3635 (X = O)	Not observed	Not observed	Not observed
	3405 (X = N)	−40	−65	−390
a5HIH$^+$(C4)	3598 (X = O)	−63	−118	−583
	3478 (X = N)	−24	−68	−348
s5HIH$^+$(C4)	3584 (X = O)	−49	−131	−569
	3478 (X = N)	−13	−68	−348

[a] Values correspond to Ne-tagged PhH$^+$(O)–Ne(OH),[20] which closely approximate those of bare PhH$^+$(O). Complexation-induced red-shifts are calculated relative to PhH$^+$(O)–Ne(OH). [b] Value corresponds to π-bonded PhH$^+$(o/p)–Ar(π),[20] which closely approximates that of bare PhH$^+$(o/p). [c] Values calculated at the B3LYP-D3/aug-cc-pVTZ level. [d] Values taken from ref. 14.

protomers for 5HIH$^+$, namely, s/a5HIH$^+$(C3), s/a5HIH$^+$(C4), and s/a5HIH$^+$(O).

In the neutral ground state (S$_0$), NH- and OH-bound hydrates of both s- and a5HI rotamers could be identified by isomer-selective IR spectroscopy.[56] While neutral a5HI–W clusters are more stable by $\Delta E_0 > 1.1$ kJ mol^{-1}, protonation reverses this trend, such that protonated s5HIH$^+$–W are more stable by $\Delta E_0 > 1.5$ kJ mol^{-1}. In the S$_0$ state, OH···W bonds are stronger than NH···W bonds. Upon C3-protonation the neutral NH···W bond is strengthened from $D_e = 40.2$ to 88.6 kJ mol^{-1}.[5] The strengthening of the OH···W bond is less pronounced with $D_e = 43.3$ vs. 76.8 kJ mol^{-1}.[5] These results were rationalized by the large charge density on the pyrrole ring of 5HIH$^+$(C3), which affects the acidity of the OH and NH groups. Our recent analysis of the NBO charge distribution in 5HIH$^+$(C3), 5HIH$^+$(C4), and 5HIH$^+$(O) quantifies this qualitative argument.[17]

The IRPD spectrum of 5HI$^+$–W is depicted in Fig. 3. Number and positions of the bands (A–F) are similar to those observed for 5HIH$^+$–W, indicating comparable structures of the 5HI core and similar microhydration motifs (OH···W and NH···W H-bonds). However, band widths and intensities differ significantly. The spectrum of 5HI$^+$–W was explained by the coexistence of 5HI$^+$–W(OH) and 5HI$^+$–W(NH).[23] Also in the cationic ground state (D$_0$), OH···W bonds are stronger than NH···W bonds, yet the interaction strengths are significantly enhanced compared to the neutral clusters. Hence, OH···W bonds are strongly preferred over NH···W bonds by a factor of 10.[23] A very rough estimate of the population of the 5HIH$^+$–W protomers yields that 5HIH$^+$(C3)–W(NH) and 5HIH$^+$(C4)–W(OH) contribute ≈70%, 5HIH$^+$(C4)–W(NH) ≈20%, and 5HIH$^+$(O)–W(OH) ≈10%. Thus, due to the strong variation of the acidity of the NH and OH groups upon protonation, there is no longer any preference for OH···W or NH···W bonds. In the D$_0$ state, clusters of s5HI$^+$ are more stable than those of a5HI$^+$, and the same is true for the protonated species.

IRPD spectroscopy of 5HI$^+$–W$_n$ clusters reveals the competition between interior ion solvation and the formation of H-bonded water networks.[23] For 5HI$^+$–W$_2$, interior ion solvation at both acidic groups (OH/NH) is strongly preferred (≥90%). For 5HI$^+$–W$_3$, two isomers coexist which bear one single W and one W$_2$ dimer H-bonded to either of the functional groups. The IRPD spectrum of 5HI$^+$–W$_3$ suggests a strong preference for attachment of the W$_2$ dimer at the OH group, leading to an estimated population ratio of 10 : 1 for OH/W/NH : OH/NH/W.[23] Proton transfer from 5HI$^+$–W$_n$ to the solvent was not observed for $n \leq 3$. These results are in line with our current findings on the 5HIH$^+$–W$_n$ clusters.

3.8 Comparison to PhH$^+$–W$_n$

It is instructive to compare our results for 5HIH$^+$–W$_n$ to those obtained by IRPD spectroscopy of the related PhH$^+$–W$_n$ clusters because (i) similar protonation mechanisms have been evidenced for PhH$^+$, resulting in carbenium PhH$^+$(p/o) and oxonium PhH$^+$(O) ions,[14,18–20,24] and (ii) as a consequence, the micro-hydration is expected to be similar. In our previous study,[17] we compared the protonation of 5HIH$^+$ and PhH$^+$ and their micro-solvation by Ar and N$_2$, revealing that the acidity of the OH group increases as s5HIH$^+$(C3) < a5HIH$^+$(C4) < s5HIH$^+$(C4) < PhH$^+$(p/o) < s5HIH$^+$(O) < a5HIH$^+$(O) < PhH$^+$(O).[17] The acidity of the functional group(s) correlates with the H-bond strength and is crucial for proton transfer.

The IRPD spectra of PhH$^+$–W$_n$ with $n \leq 5$ were interpreted by PhH$^+$(p/o)–W$_n$ and PhH$^+$(O)–W$_n$ clusters, for which proton transfer occurs at different critical sizes of the hydration shell (n_c). In the case of PhH$^+$(O)–W$_n$, the critical size is determined as $n_c = 3$, and for PhH$^+$(o/p)–W$_n$ as $n_c = 4$.[14] Most likely, the transferred proton is the excess proton, coming from the OH$_2$ group of PhH$^+$(O) and the CH$_2$ group of PhH$^+$(p/o). However, for all PhH$^+$–W$_n$ exclusively the OH group is solvated. Hence, the W$_n$ network has to bridge the OH group and the protonated CH$_2$ group in PhH$^+$(p/o) which is only possible for W$_{n \geq 4}$ chains. Our current IRPD spectra of 5HIH$^+$–W$_n$ do not indicate proton transfer at $n \leq 3$ for any of the assigned protomers. This finding is interesting as we also observe hydrated oxonium ions, 5HIH$^+$(O)–W$_n$. To elucidate the microsolvation mechanism, we compare the acidity of the OH groups of PhH$^+$(o/p) and PhH$^+$(O) to those of the observed 5HIH$^+$(C3), 5HIH$^+$(C4), and 5HIH$^+$(O) clusters with the aid of the measured complexation-induced red-shifts of the OH stretch ($\Delta\nu_{OH}$) (Table 2). Most obviously, the acidity of the OH group of 5HIH$^+$(C3) is the smallest, because its ν_{OH} has the highest measured frequency (3635 cm^{-1}),[17] and we do not observe OH···W bonds for 5HIH$^+$(C3)–W. Preferentially, s/a5HIH$^+$(C4) are solvated at the OH group, yet the observed $\Delta\nu_{OH}$ shifts are of medium size ($\Delta\nu_{OH} = -569/-583$ cm^{-1}). The OH···W H-bond in PhH$^+$(o/p)–W is comparably strong with $\Delta\nu_{OH} = -654$ cm^{-1}. Unfortunately, $\Delta\nu_{OH}$ has not been measured for PhH$^+$(O)–W,[14] but is estimated to be larger than -877 cm^{-1}. Hence, we determine the largest value of $\Delta\nu_{OH} = -1304$ cm^{-1} for a/s5HIH$^+$(O)–W. Considering the red-shifts induced by attachment of Ar and N$_2$ at the OH group of PhH$^+$(O) and 5HIH$^+$(O), we again infer a somewhat

larger acidity of the OH group of PhH$^+$(O).[17] Hence, proton transfer may occur at $n_c \geq 4$ for 5HIH$^+$(O)–W$_n$.

4. Conclusions

Herein, we investigate the initial microhydration of a prototypical protonated heteroaromatic biomolecule using IRPD spectroscopy of size-selected 5HIH$^+$–W$_n$ (W = H$_2$O, n = 1–3) clusters in the XH stretching range and calculations at the B3LYP-D3/aug-cc-pVTZ level. Our results may be summarized as follows.

We observe clusters of the C3- and C4-protonated carbenium ions, 5HIH$^+$(C3) and 5HIH$^+$(C4), and the oxonium ion, 5HIH$^+$(O). Detection of 5HIH$^+$(O)–W$_n$ clusters is surprising at first glance because they are significantly less stable ($\Delta E_0 > 75$ kJ mol^{-1}). However, the H-bonds to the protonated OH$_2$ group are very strong ($D_0 > 99$ kJ mol^{-1}). In line with our previous results obtained for 5HIH$^+$–L with L = Ar and N$_2$,[17] 5HIH$^+$(O)–W$_n$ clusters benefit from the strong OH$\cdots$W bond and the twofold degeneracy of the corresponding minimum. At the current spectral resolution, *syn* and *anti* rotamers (*s*- and *a*5HIH$^+$) are not distinguishable. As the energy differences between their clusters are rather small ($\Delta E_0 = 1$–5 kJ mol^{-1}), we assume the production of both *s*- and *a*5HIH$^+$–W$_n$ clusters.

5HIH$^+$–W$_n$ grow by H-bonding of the first W ligand to the acidic NH and OH groups, and π-stacking of W is unlikely. The absolute and relative strengths of the NH$\cdots$W and OH$\cdots$W H-bonds strongly depend on the 5HIH$^+$ protomer. The strongest H-bond is found in 5HIH$^+$(O)–W(OH) with W attached to one of its OH groups with an outstandingly high binding energy of $D_0 = 99.3$ kJ mol^{-1}. The acidity of the OH group (NH group) increases (decreases) in the order 5HIH$^+$(C3) < 5HIH$^+$(C4) < 5HIH$^+$(O).[17] Thus, we predominantly observe 5HIH$^+$(C3)–W(NH), both 5HIH$^+$(C4)–W(NH) and 5HIH$^+$(C4)–W(OH), and 5HIH$^+$(O)–W(OH) clusters. IRPD spectra of tagged 5HIH$^+$–W–Ar/N$_2$ clusters confirm this assignment. Interior ion solvation and formation of water networks compete for 5HIH$^+$–W$_2$. We assign carbenium clusters with both functional groups solvated, *s*5HIH$^+$(C3)–W$_2$(NH–OH) and *s*5HIH$^+$(C4)–W$_2$(NH–OH), and those with W$_2$ water chains at their respective most acidic functional group, *s*5HIH$^+$(C3)–W$_2$(NH–W) and *s*5HIH$^+$(C4)–W$_2$(OH–W). The IRPD spectrum of 5HIH$^+$–W$_2$ does not clearly show features of any 5HIH$^+$(O)–W$_2$ clusters. The spectrum of 5HIH$^+$–W$_3$ clearly indicates W$_2$ water chains at the NH and OH groups. It can readily be explained by the two most stable carbenium ions, *s*5HIH$^+$(C3)–W$_3$(OH–NH–W) and *s*5HIH$^+$(C4)–W$_3$(OH–W–NH). Isomer *s*5HIH$^+$(C3)–W$_3$(W–NH–W) with a bifurcated H-bond may also contribute to the measured spectrum. Again, we exclude the oxonium 5HIH$^+$(O)–W$_3$ clusters. Future IR-UV or IR-IR double resonance spectroscopy may facilitate disentangling the isomer contribution to the IRPD spectrum of 5HIH$^+$–W$_n$.

Compared to the growth of 5HIH$^+$–L$_n$ clusters (L = Ar, N$_2$), H-bonding is strongly preferred for L = W, and W$_n$ networks compete with interior ion solvation, which is not the case for L = Ar/N$_2$. The strength of individual H-bonds increases in the order Ar < N$_2$ < W as shown by comparison of the respective complexation-induced frequency red-shifts ($\Delta\nu_{XH}$) of the corresponding H-bonded proton donor stretching modes.

Protonation significantly strengthens the OH$\cdots$W and NH$\cdots$W H-bonds observed in neutral 5HI–W due to the excess charge.[5] The distribution of the excess positive charge is very different in the individual protomers directly affecting the acidity of the OH and NH groups. In the neutral S$_0$ ground state, *a*5HI–W clusters are more stable than *s*5HI–W.[56] In contrast, ionization into the D$_0$ state and protonation reverse the relative stability of the rotamers.[22,23] The mechanism of the growth of the initial solvation shell ($n < 4$) is very similar for cationic and protonated hydrates.

IRPD spectra of the PhH$^+$ subunit of 5HIH$^+$ revealed proton transferred at critical sizes $n_c = 3$ and 4 in the case of PhH$^+$(O)–W$_n$ and PhH$^+$(o/p)–W$_n$, respectively.[14] In contrast, we do not observe any clear characteristics of proton-transferred structures in the 5HIH$^+$–W$_n$ clusters up to $n = 3$. Yet, we observe an increase in the acidity of the OH group in the order 5HIH$^+$(C3) < 5HIH$^+$(C4) < PhH$^+$(p/o) < 5HIH$^+$(O) < PhH$^+$(O). Hence, proton transfer may occur at $n_c \geq 4$ for 5HIH$^+$(O)–W$_n$.

Conflicts of interest

There are no conflicts to declare.

Acknowledgements

References

1 A. T. Balaban, D. C. Oniciu and A. R. Katritzky, *Chem. Rev.*, 2004, **104**, 2777–2812.

2 J. M. Berg, J. L. Tymoczko and L. Stryer, *Biochemistry*, Freeman, New York, 2002.

3 J. P. Schermann, *Spectroscopy and modeling of biomolecular building blocks*, Elsevier, 2007.

4 H.-S. Andrei, N. Solcà and O. Dopfer, *ChemPhysChem*, 2006, **7**, 107–110.

5 R. Omidyan, M. Omidyan and A. Mohammadzadeh, *RSC Adv.*, 2016, **6**, 33148–33158.

6 E. P. L. Hunter and S. G. Lias, *J. Phys. Chem.*, 1998, **27**, 413–656.

7 D. J. Goebbert and P. G. Wenthold, *Eur. J. Mass Spectrom.*, 2004, **10**, 837–845.

8 M. Miyazaki, A. Fujii, T. Ebata and N. Mikami, *Chem. Phys. Lett.*, 2004, **399**, 412–416.

9 E. S. Kryachko and M. T. Nguyen, *J. Phys. Chem. A*, 2001, **105**, 153–155.

10 T. C. Cheng, B. Bandyopadhyay, J. D. Mosley and M. A. Duncan, *J. Am. Chem. Soc.*, 2012, **134**, 13046–13055.

11 I. Alata, M. Broquier, C. Dedonder-Lardeux, C. Jouvet, M. Kim, W. Y. Sohn, S. Kim, H. Kang, M. Schütz and A. Patzer, *et al.*, *J. Chem. Phys.*, 2011, **134**, 74307.

12 O. Dopfer, A. Patzer, S. Chakraborty, I. Alata, R. Omidyan, M. Broquier, C. Dedonder and C. Jouvet, *J. Chem. Phys.*, 2014, **140**, 124314.

13 O. Dopfer and M. Fujii, *Chem. Rev.*, 2016, **116**, 5432–5463.

14 M. Katada and A. Fujii, *J. Phys. Chem. A*, 2018, **122**, 5822–5831.

15 K. Tanabe, M. Miyazaki, M. Schmies, A. Patzer, M. Schütz, H. Sekiya, M. Sakai, O. Dopfer and M. Fujii, *Angew. Chem., Int. Ed.*, 2012, **51**, 6604–6607.

16 M. Ataelahi and R. Omidyan, *J. Phys. Chem. A*, 2013, **117**, 12842–12850.

17 J. Klyne and O. Dopfer, *J. Phys. Chem. B*, 2018, **122**, 10700–10713.

18 N. Solcà and O. Dopfer, *Chem. Phys. Lett.*, 2001, **342**, 191–199.

19 N. Solcà and O. Dopfer, *J. Chem. Phys.*, 2004, **120**, 10470–10482.

20 N. Solcà and O. Dopfer, *J. Am. Chem. Soc.*, 2004, **126**, 1716–1725.

21 S. A. Nizkorodov, O. Dopfer, T. Ruchti, M. Meuwly, J. P. Maier and E. J. Bieske, *J. Phys. Chem.*, 1995, **99**, 17118–17129.

22 J. Klyne and O. Dopfer, *J. Mol. Spectrosc.*, 2017, **337**, 124–136.

23 J. Klyne, M. Miyazaki, M. Fujii and O. Dopfer, *Phys. Chem. Chem. Phys.*, 2018, **20**, 3092–3108.

24 N. Solcà and O. Dopfer, *J. Chem. Phys.*, 2004, **121**, 769–772.

25 O. Dopfer, *Int. Rev. Phys. Chem.*, 2003, **22**, 437–495.

26 O. Dopfer, *Z. Phys. Chem.*, 2005, **219**, 125–168.

27 M. J. Frisch, *et al.*, *GAUSSIAN09, Rev. D.01*, Gaussian, Inc., Wallingford, CT, 2009.

28 J. Klyne, A. Bouchet, S. Ishiuchi, M. Fujii, M. Schneider, C. Baldauf and O. Dopfer, *Phys. Chem. Chem. Phys.*, 2018, **20**, 28452–28464.

29 W. Fu and W. S. Hopkins, *J. Phys. Chem. A*, 2017, **122**, 167–171.

30 M. Rossi and C. Baldauf, *J. Phys.: Condens. Matter*, 2015, **27**, 493002.

31 A. D. Becke, *Phys. Rev. A: At., Mol., Opt. Phys.*, 1988, **38**, 3098.

32 A. D. Becke, *J. Chem. Phys.*, 1993, **98**, 5648–5652.

33 C. Lee, W. Yang and R. G. Parr, *Phys. Rev. B: Condens. Matter Mater. Phys.*, 1988, **37**, 785.

34 T. H. Dunning, *J. Chem. Phys.*, 1989, **90**, 1007–1023.

35 M. Miyazaki, A. Naito, T. Ikeda, J. Klyne, K. Sakota, H. Sekiya, O. Dopfer and M. Fujii, *Phys. Chem. Chem. Phys.*, 2018, **20**, 3079–3091.

36 M. Schütz, Y. Matsumoto, A. Bouchet, M. Öztürk and O. Dopfer, *Phys. Chem. Chem. Phys.*, 2017, **19**, 3970–3986.

37 Q. Zhang and L. Du, *Comput. Theor. Chem.*, 2016, **1078**, 123–128.

38 H. Zhao, J. Chang and L. Du, *Comput. Theor. Chem.*, 2016, **1084**, 126–132.

39 S. Grimme, J. Antony, S. Ehrlich and H. Krieg, *J. Chem. Phys.*, 2010, **132**, 154104.

40 M. Miyazaki, A. Fujii and N. Mikami, *J. Phys. Chem. A*, 2004, **108**, 8269–8272.

41 K. Chatterjee and O. Dopfer, *Phys. Chem. Chem. Phys.*, 2017, **19**, 32262–32271.

42 B. E. Rocher-Casterline, L. C. Ch'ng, A. K. Mollner and H. Reisler, *J. Chem. Phys.*, 2011, **134**, 211101.

43 K. Chatterjee and O. Dopfer, *Chem. Sci.*, 2018, **9**, 2301–2318.

44 C. Baldauf, K. Pagel, S. Warnke, G. von Helden, B. Koksch, V. Blum and M. Scheffler, *Chem. – Eur. J.*, 2013, **19**, 11224–11234.

45 V. Scutelnic, M. A. S. Perez, M. Marianski, S. Warnke, A. Gregor, U. Rothlisberger, M. T. Bowers, C. Baldauf, G. von Helden and T. R. Rizzo, *et al.*, *J. Am. Chem. Soc.*, 2018, **140**, 7554–7560.

46 M. Ropo, M. Schneider, C. Baldauf and V. Blum, *Sci. Data*, 2016, **3**, 160009.

47 S. Simon, M. Duran and J. J. Dannenberg, *J. Chem. Phys.*, 1996, **105**, 11024–11031.

48 S. F. Boys and F. Bernardi, *Mol. Phys.*, 1970, **19**, 553–566.

49 G. Herzberg, *Molecular spectra and molecular structure*, Read Books Ltd, 2013.

50 V. Barone, *J. Chem. Phys.*, 2004, **122**, 14108.

51 J. Klyne, M. Schmies, M. Miyazaki, M. Fujii and O. Dopfer, *Phys. Chem. Chem. Phys.*, 2018, **20**, 3148–3164.

52 J. Klyne, M. Schmies, M. Fujii and O. Dopfer, *J. Phys. Chem. B*, 2015, **119**, 1388–1406.

53 N. Solcà and O. Dopfer, *Chem. Phys. Lett.*, 2001, **347**, 59–64.

54 O. Couronne and A. Ellinger, *Chem. Phys. Lett.*, 1999, **306**, 71–77.

55 E. A. Colbourn and A. E. Douglas, *J. Chem. Phys.*, 1976, **65**, 1741–1745.

56 T. Ikeda, K. Sakota and H. Sekiya, *J. Phys. Chem. A*, 2016, **120**, 1825–1832.